CrossMark

Experimental and Theoretical Studies on the Corrosion Inhibition Performance of Molecules Containing Tert-Butyl Benzyl Group on Mild Steel in Acid Media

Turuvekere Krishnamurthy Chaitra[1,3] · Kikkeri Narasimhashetty Mohana[1] · Harmesh Chander Tandon[2]

Abstract

The inhibition by (4-tert-butyl-phenyl)-acetic acid hydrazide (TPAH), 5-(4-tert-butyl-benzyl)-[1,3,4] oxadiazole-2-thiol (TBOT) and 5-(4-tert-butyl-benzyl)-4H-[1,2,4] triazole-3-thiol (TBTT) of mild steel corrosion in 0.5 M HCl was investigated using gravimetric and electrochemical techniques. These inhibitors acted more effectively at higher concentration and at lower temperature; among these TBTT being the most efficient inhibitor, which showed highest efficiency of 92.6% at 303 K and 4.8 mM concentration. Adsorption of TPAH followed Freundlich isotherm, whereas TBOT and TBTT followed Langmuir isotherm. Energy of activation for corrosion increased after the addition of inhibitors. Free energy of adsorption showed that all the three inhibitors get adsorbed to the mild steel surface by both physical and chemical processes. EIS studies confirmed that all the inhibitors offered higher charge transfer resistance to the corrosion current and this led to decreased double-layer capacitance. Polarization studies showed that all inhibitors emerged as mixed type. Surface studies confirmed that the pits caused by corrosion were decreased by protective film of inhibitors. Corelation of experimental data with quantum chemical parameters like E_{LUMO}, energy gap, dipole moment, hardness and softness confirmed the superior performance of TBTT as compared to TPAH and TBOT.

Keywords Mild steel · Corrosion · Adsorption · Electrochemical · Quantum chemical

1 Introduction

Designing of suitable inhibitors to corrosion of mild steel (MS) is getting higher priority because problems arising due to corrosion have greater impact on economy and safety. Retardation of corrosion attack on MS during industrial processes such as pickling, cleaning and descaling can be done through addition of small amount of inhibitors to the acid solution being used. By influencing kinetics of electrochemical reactions of corrosion process, inhibitors retard the metal corrosion. Although many kinds of inhibitors are used to control metal corrosion in acidic environment, organic inhibitors containing heteroatom such as O, N, S, and P are found to have particular use due to higher basicity and electron donating ability. Inhibitors which possess electron-rich functional groups (>C=N, –C=O, –N=N–, –NR₂, –OH, –RCH₃, –SH, –OCH₃, –C=C<) and aromatic electrons have higher tendency to adsorb onto the metal surface [1]. Many organic compounds containing electron-releasing groups like methoxy [2], butyl [3], butoxy [4], hydroxy [5] and amino [6] groups have been previously reported as corrosion inhibitors for mild steel. So, molecules containing tertiary butyl benzyl group can be effectively used as inhibitors for the corrosion of mild steel in acid medium.

The present investigation is aimed to find out the corrosion inhibition capability of hydrazide, oxadiazole and triazole moieties using experimental and quantum chemical methods. The motive in selecting these inhibitors is that they possess good number of nitrogen atoms, aromatic rings and electron donating tertiary methyl and thiol groups. It is clear from review of literature that all three selected compounds have extensive background in controlling metal corrosion.

✉ Kikkeri Narasimhashetty Mohana
   drknmohana@gmail.com

1   Department of Studies in Chemistry, Manasagangotri, University of Mysore, Mysuru, Karnataka 570006, India

2   Department of Chemistry, Sri Venkateswara College, Dhaula Kuan, New Delhi 110021, India

3   Department of Studies in Chemistry, Pooja Bhagavat Memorial Mahajana PG Centre, Mysuru 570003, India

Some aromatic hydrazides like salicylic acid hydrazide and cinnamic acid hydrazide were tested as MS corrosion inhibitors in HCl media and very good efficiency of 93% was obtained [7]. *N*-phenyl oxalic dihydrazide was synthesized and tested as corrosion inhibitor for MS in acid media to get inhibition efficiency up to 79% [8]. The influence of three oxadiazole derivatives on the corrosion inhibition of steel in 2 M H_3PO_4 solution was studied to get maximum inhibition of 76% [9]. MS corrosion inhibition activity of triazole derivatives was investigated in 5% HCl to get excellent inhibition of 95% [10]. New pyridine based 1,3,4-oxadiazole derivatives were synthesized and established as MS corrosion inhibitors with maximum efficiency of 89% [11] Some synthesized triazole Schiff bases were checked for MS corrosion inhibition to get maximum inhibition efficiency of 90% in our previous study [12].

In continuation of our previous work, the present study reports the synthesis, characterization and corrosion inhibition ability of molecules containing hydrazide, oxadiazole and triazole moieties on MS in 0.5 M HCl using gravimetric and electrochemical techniques. Surface morphology was studied by scanning electron microscope (SEM). As charge transfer is one of the important criterion of corrosion reaction, quantum chemical parameters like energy of highest occupied molecular orbital (E_{HOMO}), energy of lowest unoccupied molecular orbital (E_{LUMO}), energy gap (ΔE), dipole moment (μ), electron affinity (A), hardness (η) and softness (σ) were calculated and correlated.

2 Experimental

2.1 Materials and Sample Preparation

MS specimens with composition (wt%): C—0.051; Mn—0.179; Si—0.006; P—0.005; S—0.023; Cr—0.051; Ni—0.05; Mo—0.013; Ti—0.004; Al—0.103; Cu—0.050; Sn—0.004; B—0.00105; Co—0.017; Nb—0.012;

Pb—0.001 and remaining being Fe was used. Dimension of the specimens used was 2 cm×2 cm×0.1 cm and 5 cm×2 cm×0.1 cm for gravimetric and electrochemical experiments, respectively. MS specimens used were abraded with SiC emery papers of different grades, degreased with acetone and dried with clean tissue paper. For EIS and polarization studies, the MS specimens were implanted in epoxy resin and a geometrical surface area of 1 cm^2 was exposed to the electrolyte. Experiments were conducted in 1.2–4.8 mM concentration range using 0.5 M HCl. Veego Melting Point VMP III apparatus was used to find the melting range of the inhibitors.

2.2 Synthesis of Inhibitors

Scheme for the synthesis of TPAH, TBOT and TBTT is outlined in Fig. 1.

2.2.1 Synthesis of (4-Tert-Butyl-Phenyl)-Acetic Acid Ethyl Ester (Compound 2)

Syntheses of compounds 2 and 3 were done as reported earlier [13]. A mixture of 10 mM (4-isopropyl-phenyl)-acetic acid (compound 1) and 0.2 mL of concentrated sulfuric acid in 20 mM ethanol was refluxed for 10 h. Completion of esterification reaction was checked by TLC. Reaction mixture (RM) was concentrated, diluted with water and extracted with ethyl acetate. Organic layer was washed with saturated sodium bicarbonate solution followed by brine, dried over sodium sulfate and evaporated to get compound 2 which was recrystallized and stored.

2.2.2 Synthesis of (4-Tert-Butyl-Phenyl)-Acetic Acid Hydrazide (Compound 3(TPAH))

Ten mM of (4-tert-butyl-phenyl)-acetic acid ethyl ester and 25 mM hydrazine hydrate were taken in ethanol and heated under reflux for 6 h. Completion of the reaction was checked

Fig. 1 Scheme for the synthesis of inhibitors
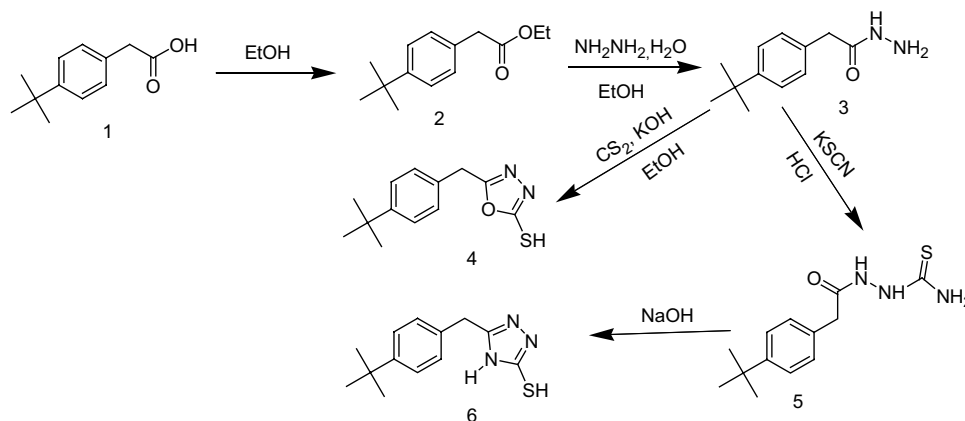
by TLC; RM was concentrated, poured into 200 mL ice-cold water. Solid formed was collected by filtration and recrystallized from ethanol to get compound 3 in pure form.

2.2.3 Synthesis of 5-(4-Tert-Butyl-Benzyl)-[1,3,4] Oxadiazole-2-Thiol (Compound 4 (TBOT))

Compound 4 was synthesized as reported [14]. To 10 mM compound 3 solution in ethanol (20 mL), 10 mM potassium hydroxide in water (5 mL) and 30 mM carbon disulfide were added. The RM was heated under reflux till hydrogen sulfide evolution ceased (around 15 h). It was cooled, diluted with ice-cold water and acidified with 10% HCl. Solid separated out was filtered, washed and recrystallized from ethanol to get the pure form. Melting range of the product was 187–189 °C and yield was 90%.

2.2.4 Synthesis of 1-Tert-Butyl-Methyl-Benzyl Thiosemicarbazide (Compound 5)

Syntheses of compounds 5 and 6 were done as per reported literature [15]. Compound 5 was prepared by refluxing a suspension of compound 3 (10 mM) and potassium thiocyanate (20 mM) in HCl (5 mL) and water (100 mL) for 3 h. Completion of the reaction was checked by TLC. After cooling the mixture, white solid was separated. The solid separated was filtered, dried and recrystallized from ethanol to get pure compound.

2.2.5 Synthesis of 5-(4-Tert-Butyl-Benzyl)-4H-[1,2,4] Triazole-3-Thiol (Compound 6(TBTT))

Compound 5 (10 mM) was refluxed in 5% of 50 mL NaOH for 3 h. Completion of the reaction was checked by TLC. RM was neutralized with HCl to pH 5–6. Compound 6 was obtained as white solid which was filtered, dried and recrystallized from ethanol. Melting range of the product was 209–211 °C, and yield was 94%.

2.2.6 Spectral Data

(*4-tert-butyl-phenyl*)-*acetic acid hydrazide* (*TPAH*): IR (cm^{-1}) 1465–1517 (Ar C=C), 1634 (NH), 2960 {(CH$_3$)$_3$C}, 3313 (NH$_2$). ^{1}H NMR (400 MHz, DMSO-d$_6$) δ ppm: 1.72 (s, 9H, 3×CH$_3$), 2.870 (d, 2H, NH$_2$), 4.14 (s, 2H, CH$_2$), 7.45 (m, 2H, ArH), 7.65 (m, 2H, ArH), 7.87 (s, 1H, NH). MS: 206 (M +), 207 (M + 1).

5-(4-Tert-Butyl-benzyl)-[1,3,4] oxadiazole-2-thiol (*TBOT*): IR (cm^{-1}) 1516 (Ar C=C), 2963 (R$_3$C), 1175 (C=S) ^{1}H NMR (400 MHz, DMSO-d$_6$) δ ppm: 1.29 (s, 9H, 3×CH$_3$), 2.17 (s, 1H, SH), 3.61 (s, 2H, CH$_2$), 7.22–7.20 (m, 2H, Ar–H), 7.36–7.34. (m, 2H, ArH). ^{13}C-NMR (100 MHz,

DMSO) δ ppm: 31.3, 34.4, 40.5, 125.5, 129.01, 130.2, 150.2, 177.9. MS: 249 (M + 1), 250.09 (M + 2).

5-(4-tert-Butyl-benzyl)-4H-[1,2,4] triazole-3-thiol (*TBTT*): IR (cm^{-1}) 1477 (Ar C=C), 2964 ((CH$_3$)$_3$C), 1196 (C=S) ^{1}H NMR (400 MHz, DMSO-d$_6$) δ ppm: 1.25 (s, 9H, 3×CH$_3$), 3.30 (s, 1H, SH), 4.06 (s, 2H, CH$_2$), 7.22 (d, 2H, ArH, J = 7.04 Hz), 7.36 (d, 2H, ArH, J = 7.12 Hz), 14.38 (s, 1H, NH). MS: 248.10 (M + 1), 249.03 (M + 2).

2.3 Weight Loss Measurements

MS specimens were immersed in 0.5 M HCl without and with varying amounts of the inhibitors for 6 h in a thermostatically controlled water bath at constant temperature, under aerated condition (Weber limited, Chennai, India). The specimens were removed after 6 h of immersion, rinsed with water followed by drying with acetone. Weight loss of three specimens was determined by analytical balance (Sartorius, precision ± 0.1 mg), and the mean was calculated.

2.4 Electrochemical Measurements

Potentiodynamic polarization and EIS experiments were carried out using CHI660D electrochemical workstation. The traditional three-electrode cell consisting of silver/silver chloride reference electrode, a platinum auxiliary electrode and the working MS electrode with 1 cm^2 exposed areas was used. Specimens were treated in the way similar to gravimetric measurements. For polarization and impedance measurements, the MS specimens were inserted in epoxy resin to expose a geometrical surface area of 1 cm^2 to the electrolyte. Potentiodynamic polarization measurements were recorded by changing the electrode potential from − 200 to + 200 mV, related to the open-circuit potential, with the scanning rate of 10 mV s^{-1}. Prior to EIS measurements, open-circuit potential was stabilized till half an hour. EIS data were recorded using AC sinusoidal signal in the frequency range 0.1–1,00,000 Hz with amplitude 0.005 V. Simulation of EIS data was done using Zsimpwin software.

2.5 Quantum Chemical Calculations

The geometrical optimization of studied compounds was done by Ab initio method at 6–31G** basis set for all atoms. For energy minimization, 1.0 convergence limit and 1.0 k cal/A mol rms gradient were kept. The Polak–Ribiere conjugate gradient algorithm which is very fast and precise was used for geometrical optimization. The HYPERCHEM 7.52 (Hypercube Inc., Florida, USA, 2003) professional software was employed for all calculations.

2.6 Scanning Electron Microscopy (SEM)

The SEM images were taken using Zeiss electron microscope with the working voltage of 15 kV, and the working distance was 10 mm. In SEM micrographs, the specimens were exposed to 0.5 M HCl in the absence and presence of three inhibitors at optimum condition after 6 h of immersion. The SEM images were taken for polished MS specimen and specimen immersed in acid solution with and without inhibitors.

3 Results and Discussion

3.1 Weight Loss Method

3.1.1 Effect of Concentration

Weight loss experiments were conducted from 303 to 333 K for 6 h at different concentrations to optimize the concentration and temperature. The results obtained are presented in Table 1. Using loss in weight of MS specimens during 6 h of immersion, corrosion rate (C_R) was calculated from formula (1) and by this inhibition efficiency [IE (%)] was determined using the formula (2)

$$C_R = \frac{\Delta W}{St} \tag{1}$$

$$IE(\%) = \frac{(C_R)_a - (C_R)_p}{(C_R)_a} \times 100 \tag{2}$$

where ΔW is the weight loss, is the surface area of the specimen (cm^2), is the immersion time (h), and $(C_R)_a$, $(C_R)_p$ are corrosion rates in the absence and presence of the inhibitor, respectively. Increase in concentration of TPAH, TBOT and TBTT led to increase in IE (%) at all temperatures. This may be due to increase in the amount of adsorbent and as also the surface area of MS due to availability of more number of molecules. Highest inhibition efficiencies of 92.6, 91.7 and 80% were recorded by TBTT, TBOT and TPAH, respectively, at 4.8 mM concentration. Electron-releasing tert-butyl group in the inhibitors increases electron density on the benzene ring thus facilitate strong binding of inhibitors to the metal surface and play pivotal role in enhancing inhibition performance of studied compounds. The presence of highly interactive nitrogen atoms, oxygen atoms and aromatic electrons in the inhibitors allowed strong adsorption on empty d-orbitals of Fe surface through available electrons. The higher inhibition efficiency of TBTT compared to TBOT is due to better electron donating capacity due to the presence of nitrogen instead of oxygen atom.

3.1.2 Activation and Thermodynamic Parameters

The influence of temperature on the inhibition characteristics was determined by conducting weight loss measurements at temperatures varying from 303 to 333 K in the absence and presence of different concentrations of TPAH, TBOT and TBTT. IE (%) of all inhibitors decreased on increasing solution temperature. The increase in C_R with temperature may be related to two factors: (1) at elevated temperatures, as the inhibitor molecules gain sufficient energy, they quickly get desorbed from MS surface resulting in shortening of time

Table 1 Weight loss data of mild steel corrosion in 0.5 M HCl in the presence of different concentrations of the inhibitors at different temperature

Inhibitor	C (mM)	30 °C C_R (mg cm^2 h^{-1})	IE (%)	40 °C C_R (mg cm^{-2} h^{-1})	IE (%)	50 °C C_R (mg cm^2 h^{-1})	IE (%)	60 °C C_R (mg cm^{-2} h^{-1})	IE (%)
	Blank	0.516	–	0.883	–	1.224	–	1.65	–
TPAH	1.2	0.297	42.4 ± 1.30	0.552	37.5 ± 0.81	0.813	33.6 ± 0.62	1.121	32.0 ± 0.87
	2.4	0.238	53.8 ± 0.76	0.458	48.1 ± 0.44	0.672	45.1 ± 0.11	0.977	40.8 ± 0.58
	3.6	0.163	68.3 ± 0.92	0.34	61.4 ± 0.85	0.55	55.0 ± 1.73	0.818	50.4 ± 1.19
	4.8	0.103	80.1 ± 0.76	0.216	75.5 ± 1.17	0.389	68.2 ± 0.51	0.640	61.2 ± 0.23
TBOT	1.2	0.082	84.2 ± 0.95	0.158	82.1 ± 0.28	0.271	77.8 ± 0.89	0.492	70.2 ± 0.66
	2.4	0.069	86.5 ± 0.37	0.141	84.0 ± 1.19	0.244	80.0 ± 0.76	0.463	71.9 ± 0.36
	3.6	0.057	89.0 ± 0.92	0.122	86.1 ± 0.06	0.212	82.7 ± 0.32	0.411	75.1 ± 0.94
	4.8	0.042	91.7 ± 0.74	0.106	88.0 ± 1.51	0.183	85.0 ± 1.68	0.350	78.7 ± 0.61
TBTT	1.2	0.076	85.1 ± 0.86	0.1503	83.0 ± 0.53	0.269	78.0 ± 1.12	0.387	76.5 ± 1.01
	2.4	0.058	88.8 ± 0.85	0.129	85.4 ± 0.71	0.246	79.9 ± 0.86	0.349	78.9 ± 1.69
	3.6	0.048	90.6 ± 0.76	0.111	87.4 ± 0.93	0.202	83.5 ± 0.065	0.298	81.9 ± 0.99
	4.8	0.038	92.6 ± 0.46	0.088	90.0 ± 0.92	0.170	86.1 ± 0.68	0.265	83.9 ± 0.73

gap between adsorption and desorption (drawing of equilibrium toward desorption) leading to longer exposure of MS surface to acidic environment. (2) Decrease in hydrogen evolution over potential resulting in acceleration of cathodic reduction.

Corrosion rate of MS and temperature of the environment can be connected by Arrhenius Eq. (3)

$$C_R = k \exp\left(-\frac{E_a^*}{RT}\right).$$ (3)

Transition state theory gives alternative form of Arrhenius equation using which enthalpy of activation and entropy of activation can be calculated

$$C_R = \frac{RT}{Nh} \exp\left(\frac{\Delta S_a^*}{R}\right) \exp\left(\frac{-\Delta H_a^*}{RT}\right)$$ (4)

where E_a^* is the energy of activation, ΔS_a^* is the entropy of activation, ΔH_a^* is the enthalpy of activation, k is Arrhenius pre-exponential factor, h is Planck's constant, N is Avogadro's number, T is the absolute temperature and R is the universal gas constant. E_a^* for investigated compounds is calculated using the slope of linear regression between ln C_R and $1/T$ (Fig. 2). ΔS_a^* and ΔH_a^* are calculated using slope and intercept of plot of ln (C_R/T) versus $1/T$, respectively (Fig. 3). Different activation parameters are listed in Table 2. Regression coefficients for TPAH, TBOT and TBTT are almost 1, thereby indicating that MS corrosion in hydrochloric acid can be elucidated using kinetic model. It is noticeable that activation energy for blank (32.1 kJ mol^{-1}) increases after the addition of inhibitors and shows increment on increasing concentration of all the three inhibitors. This indicates that as the concentration of the inhibitor in the solution becomes higher, corrosion reaction gets pushed forced to the surface sights which have got higher values of E_a^* [16]. Increase in E_a^* with increase in concentration indicates that the surface coverage is almost approaching saturation. Highest activation energy values of 51.1, 57.6, 54.3 kJ mol^{-1} were obtained for TPAH, TBOT and TBTT, respectively, at 4.8 mM. As E_a^* for the three inhibitors is below threshold value of 80 kJ mol^{-1} as required for chemisorption; however, physical adsorption is presently applicable [17]. But the type of adsorption obtained from the change of activation energy is not decisive due to competitive adsorption with water molecules; the adsorption as witnessed in the present study is a combination of physisorption and chemisorption with slight predominance of physisorption [18]. The positive values of ΔH_a^* proves the endothermic nature of MS dissolution or the dissolution of MS is difficult [19]. Addition of TPAH, TBOT and TBTT increased the ΔH_a^* from 29.5 to 48.4, 55 and 51.7 kJ mol^{-1}, respectively, indicating the enhanced difficulty for MS dissolution. Large and negative values of ΔS_a^* for TPAH, TBOT,

TBTT indicates that the formation of activated complex is an associative step or the formed activated complex is more ordered. This implies that adsorption of inhibitors in ordered fashion during the dissolution of steel. Variation of ΔH_a^* and E_a^* with concentration of inhibitors is shown Fig. 4, from which it is clear that ΔH_a^* and E_a^* vary similarly with the increase in concentration of all three inhibitors. There is gradual increase in the values of both ΔH_a^* and E_a^* with increase in concentration; therefore, reduction in MS corrosion is mainly decided by kinetic parameters of activation, and pre-exponential factor has limited significance [20].

3.1.3 Adsorption Isotherm

Primary step in the action of inhibitors in acidic medium is the adsorption onto the metal surface which involves the assumption that the corrosion reactions are prevented from occurring over the area of the metal surface covered by adsorbed inhibitor species [21, 22]. The most appropriate method to find the relation between surface coverage of an interface with the adsorbed species and concentration of an inhibitor in the solution is the study of adsorption isotherm where values of surface coverage (θ) and concentrations (C) are fitted to equations of various isotherms. In the present study, adsorption data obtained were fitted into various isotherms like Langmuir, Freundlich and Temkin isotherms. Among three studied inhibitors, TPAH fitted well in Freundlich isotherm ($R^2 = 0.9437$, 0.9972, 0.9439 for Langmuir, Freundlich and Temkin, respectively), TBOT ($R^2 = 0.9989$, 0.985, 0.9356 for Langmuir, Freundlich and Temkin, respectively) and TBTT ($R^2 = 0.9993$, 0.9864 and 0.958 for Langmuir, Freundlich and Temkin, respectively) followed Langmuir isotherm. For TPAH, according to Freundlich isotherm θ is related to C as shown below

$$\theta = K_{ads}C$$ (5)

where K_{ads} is the equilibrium constant for adsorption process. A plot of θ versus C is drawn (Fig. 5a) whose slope gave the value of K_{ads}. The value of R^2 is almost unity and intercept is around unity indicating the strong adherence of adsorption data of TPAH to Freundlich isotherm. For TBOT and TBTT, Langmuir isotherm was used to calculate adsorption parameters. According to this isotherm,

$$C/\theta = \frac{1}{K_{ads}} + C$$ (6)

Here, K_{ads} was calculated from intercept of C/θ versus C plot (Fig. 5b, c). Free energy of adsorption was calculated from K_{ads} using Eq. (7)
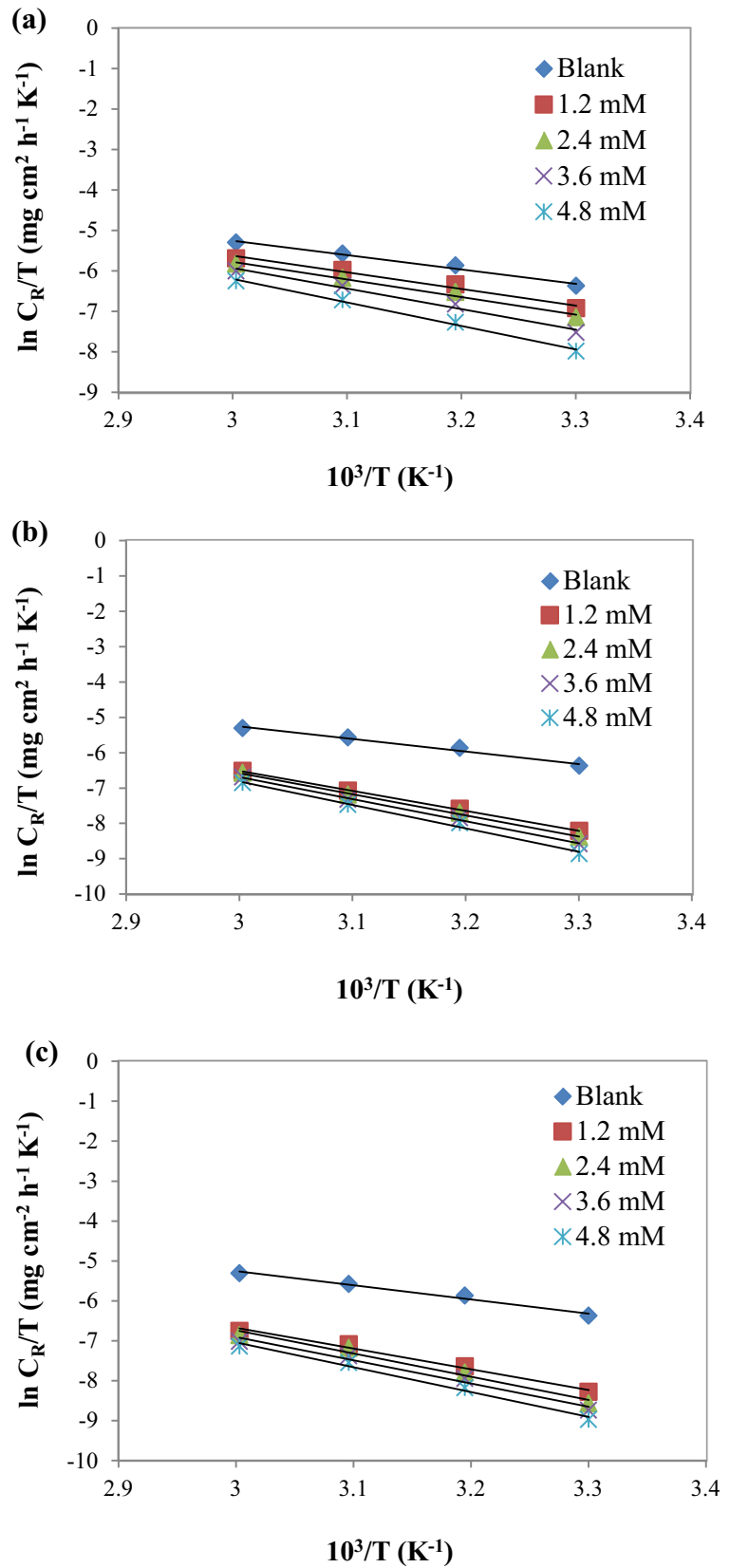
$$\Delta G_{ads}^o = -RT \ln\left(55.5K_{ads}\right)$$ (7)

where R is gas constant and T is the absolute temperature of the experiment and the constant value 55.5 is the

Fig. 2 Arrhenius plots in the absence and presence of different concentrations of **a** TPAH, **b** TBOT, **c** TBTT
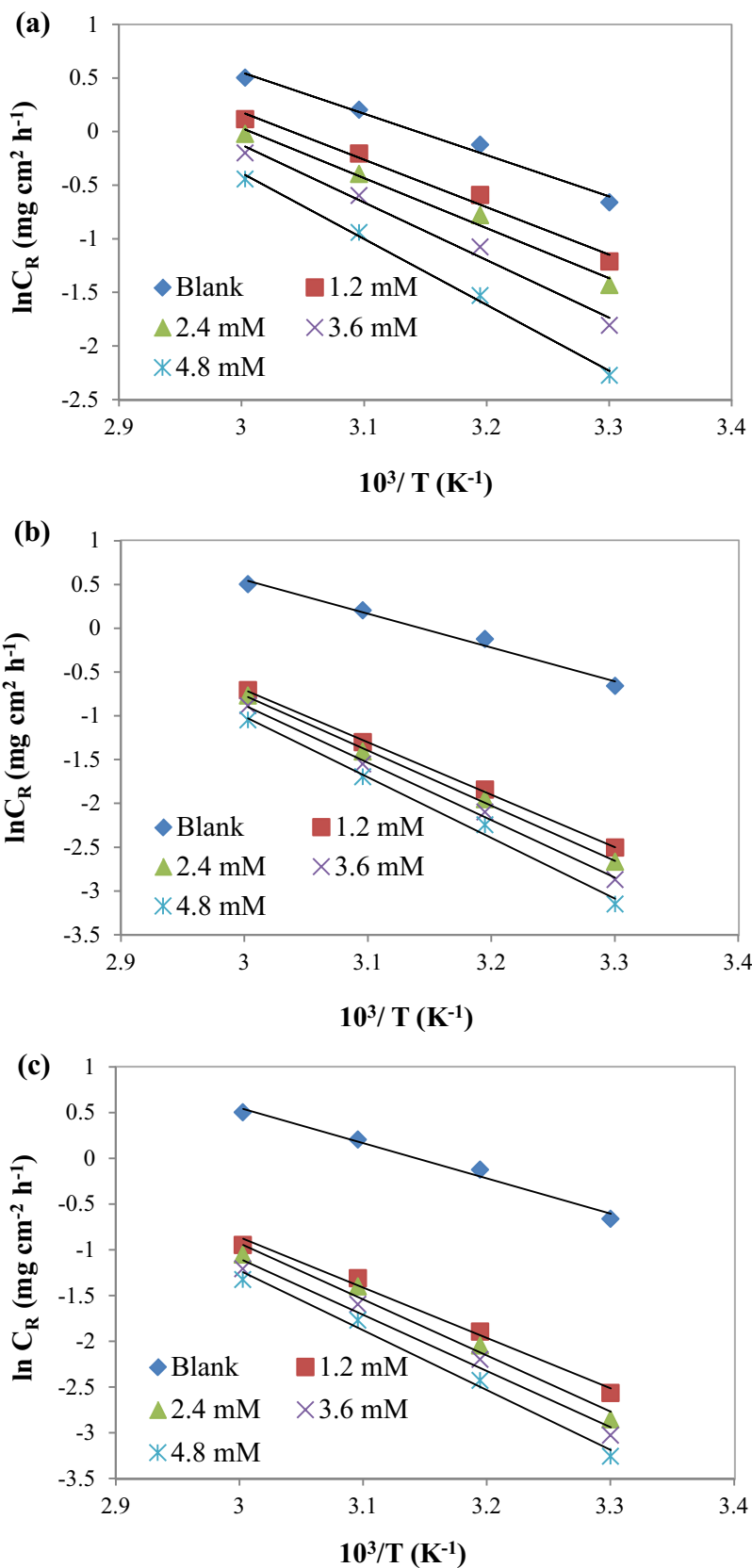
Fig. 3 Alternative Arrhenius plots in the absence and presence of different concentrations of **a** TPAH, **b** TBOT, **c** TBTT

Table 2 Activation parameters in the absence and presence of inhibitors at different concentrations

Inhibitor	C (mM)	E_a^* (kJ mol^{-1})	k (mg cm^{-2} h^{-1})	ΔH_a^* (kJ mol^{-1})	ΔS_a^* (J mol^{-1} K^{-1})
	Blank	32.1 ± 0.22	1.86×10^5	29.5 ± 0.32	-152.9 ± 0.75
TPAH	1.2	36.8 ± 0.29	7.12×10^5	34.2 ± 0.29	-141.7 ± 0.81
	2.4	38.8 ± 0.27	1.26×10^6	36.2 ± 0.27	-136.9 ± 0.78
	3.6	44.7 ± 0.26	8.99×10^6	42.1 ± 0.26	-120.6 ± 0.95
	4.8	51.1 ± 1.00	6.87×10^7	48.4 ± 0.99	-103.7 ± 2.95
TBOT	1.2	49.8 ± 0.93	3.13×10^7	47.2 ± 0.93	-110.2 ± 2.74
	2.4	52.4 ± 0.28	7.47×10^7	49.7 ± 0.28	-102.8 ± 0.67
	3.6	54.5 ± 1.13	1.50×10^7	51.9 ± 1.13	-97.4 ± 3.25
	4.8	57.6 ± 1.61	3.90×10^7	55.0 ± 1.61	-89.2 ± 4.33
TBTT	1.2	45.8 ± 0.82	6.25×10^6	43.1 ± 0.80	-123.6 ± 2.46
	2.4	50.9 ± 0.58	3.83×10^7	48.3 ± 0.34	-108.6 ± 2.07
	3.6	51.0 ± 1.28	3.28×10^7	48.4 ± 1.28	-109.8 ± 3.66
	4.8	54.3 ± 1.31	9.56×10^7	51.7 ± 1.31	-101.0 ± 3.79
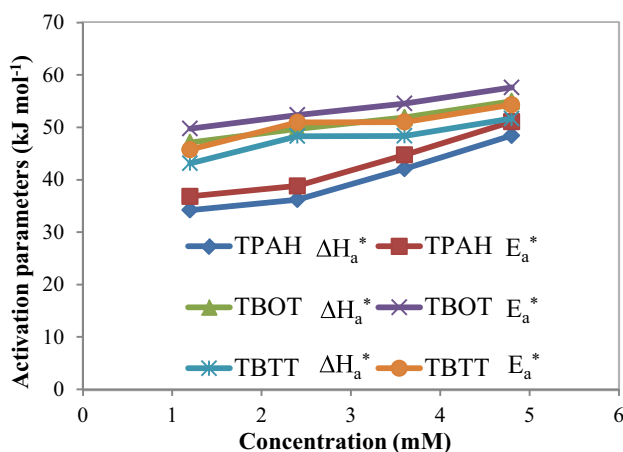
Fig. 4 Variation of activation parameters with concentration

concentration of water in solution in mol dm^{-3}. The calculated thermodynamic parameters are listed in Table 3. Free energy of adsorption for all the three inhibitors varied from -21.9 to -23.3 kJ mol^{-1} for TPAH, -31.6 to -34.6 kJ mol^{-1} for TBOT and -32.0 to -34.3 kJ mol^{-1} for TBTT. Negative value of ΔG_{ads}^o for the three inhibitors depicts spontaneity of the adsorption process and also the formation of stable adsorbed layer on the metal surface. It is well known that the values of ΔG_{ads}^o up to -20 kJ mol^{-1} are compatible with the electrostatic interaction between the charged inhibitor molecules and the charged metal surface (physisorption), and those which have higher value than -40 kJ mol^{-1} imply charge sharing or charge transfer involving coordinate bond from the inhibitor molecules to the metal surface (chemisorption) [23]. TPAH, TBOT and TBTT possess nitrogen which can undergo protonation. So, physical adsorption of charged protonated species on MS surface can takes place through chloride ions. On the other hand, chemisorption takes place independently with the help of lone pair of electrons on nitrogen atoms and aromatic electrons in the three inhibitors, whereas the presence of thiol group facilitates stronger adsorption in TBOT and TBTT. The adsorption of studied inhibitors cannot solely take place through physical or chemical means. It is a mixture involving both physisorption and chemisorption, a complex comprehensive phenomenon. As K_{ads} value indicates the strength between inhibitor and MS surface, higher values of K_{ads} obtained for TBOT and TBTT show their better adsorption capacity compared to TPAH.

Entropy of adsorption and enthalpy of adsorption process were calculated using the following thermodynamic equation:

$$\Delta G_{ads}^o = \Delta H_{ads}^o - T\Delta S_{ads}^o \tag{8}$$

The plot of ΔG_{ads}^o versus temperature (Fig. 6) gave straight line whose slope is $-\Delta S_{ads}^o$ and intercept is ΔH_{ads}^o. The negative sign of adsorption enthalpy for the three inhibitors indicates the exothermic nature of the steel dissolution process, so IE (%) decreases with temperature. According to Bentiss et al. [24], endothermic processes occur through physisorption and exothermic processes may be through physisorption or chemisorption depending upon the magnitude of ΔH_{ads}^o. It is reported that enthalpy of physisorption process is lower than 41.86 kJ mol^{-1} but the enthalpy of chemisorption process approaches 100 kJ mol^{-1} [25]. In the present study, none of the inhibitors showed ΔH_{ads}^o near 100 kJ mol^{-1}, so all the inhibitors have higher tendency to undergo physisorption. Change in ΔS_{ads}^o is the summation of solvent and solute entropy, and desorption of water results in higher solute entropy, whereas adsorption of inhibitors results in lower solvent entropy. ΔS_{ads}^o obtained for TPAH, TBOT and TBTT are positive indicating predominance of solvent entropy. It is proved that for the adsorption of inhibitors, increase in entropy is the driving force.

(a)

(b)

(c)
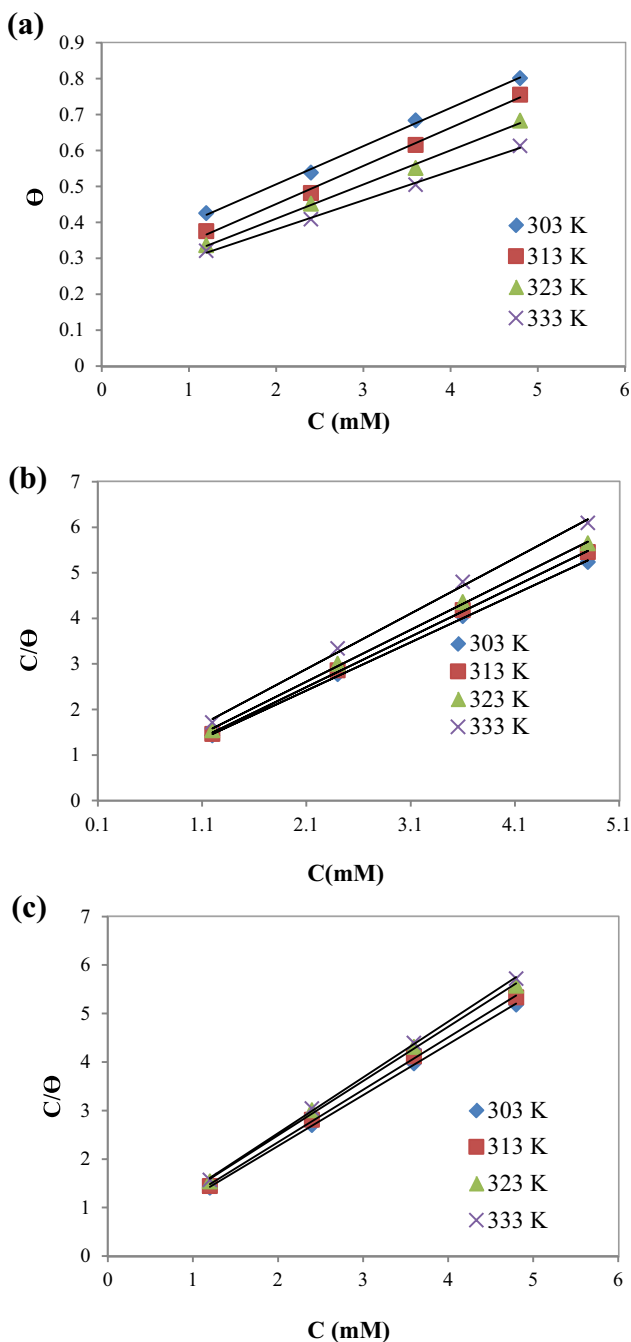
Fig. 5 Adsorption isotherm for three inhibitors, **a** Freundlich isotherm for TPAH, **b** Langmuir isotherm for TBOT, **c** Langmuir isotherm for TBTT

3.2 Electrochemical Impedance Spectroscopy (EIS)

EIS is a potent, nondestructive technique which characterizes corrosion phenomenon and protective nature of pretreatments and organic coatings over time. In EIS, sinusoidal potential excitation is applied and current signal is measured through cell and analyzed as a sum of sinusoidal

functions (a Fourier series). EIS was performed to study the corrosion behavior of MS in 0.5 M HCl at 303 K in the inhibitors, and results are expressed as Nyquist and Bode plots. Calculated impedance parameters are listed in Table 4. Nyquist plots (Figs. 7a, 8a, 9a) are characterized by single semicircles (corresponds to one time constant in Bode plots) whose diameter increases with increase in concentration of the inhibitors over the frequency range studied. The inhibitor system behaves like monolayer formation, and the dissolution process is controlled by the charge transfer reaction [26].

The depressed form of the resulting semicircle for solid electrodes is known as frequency dispersion which can be ascribed to such physical phenomena such as surface roughness, active sites, and inhomogeneity of solids [27]. Depending on the shape of complex plane impedance, data are fitted to simplest equivalent circuit (Fig. 10) consisting of polarization resistance (R_p) and constant phase element (CPE) in parallel and both in series with solution resistance (R_s). Corrosion being an electrochemical processes, corrosion also has two phases: (1) oxidation of metal (charge transfer process) and (2) diffusion of metal ions from metal surface to the solution [28]. Warburg impedance which accounts for diffusion impedance becomes unimportant because of the presence of single semicircle. Impedance curves retained their shape after the addition of TPAH, TBOT and TBTT indicating that the mechanism of inhibition is not affected. IE (%) was calculated from polarization resistance using the following formula:

$$IE(\%) = \frac{(R_p)_p - (R_p)_a}{(R_p)_p} \times 100 \qquad (9)$$

where $(R_p)_a$ and $(R_p)_p$ are the charge transfer resistance in the absence and presence of inhibitors, respectively. Polarization resistance increases from 199 Ω cm^2 (blank) after the addition of inhibitors and reaches maximum R_p of 877, 1589, 1613 Ω cm^2 at 4.8 mM for TPAH, TBOT and TBTT, respectively. This indicates the protection offered by inhibitors through barrier film MS which prevent charge and mass transfer. As there is increment in R_p, it is likely that the current has passed through the capacitor in the circuit [29]. The impedance function of a CPE can be defined as

$$Z_{CPE} = Y_o^{-1}(i\omega)^{-1} \qquad (10)$$

where Y_o is magnitude of CPE, ω is angular frequency (in rad s^{-1}), $i^2 = -1$ is the imaginary number, $n = \alpha/(\pi/2)$ in which α is the phase angle of CPE. The value of n which signifies the interphase parameter increases after the addition of the inhibitors. In case of TBOT and TBTT n increases gradually with increase in concentration but in TPAH even though n value is higher compared to blank, uniformity is not

Table 3 Thermodynamic parameters for adsorption of TPAH, TBOT and TBTT on mild steel in 0.5 M HCl at different temperatures

Inhibitor	T (K)	R^2	K_{ads} (L mol^{-1})	ΔG_{ads} (kJ mol^{-1})	ΔS_{ads} (J mol^{-1} K^{-1})	ΔH_{ads} (kJ mol^{-1})
TPAH	303	0.998 ± 0.001	106.2 ± 11.6	− 21.9 ± 0.027	46.7 ± 7.63	− 7.8 ± 2.5
	313	0.996 ± 0.0012	106.1 ± 20.03	− 22.6 ± 0.055		
	323	0.997 ± 0.0007	949.0 ± 18.4	− 23.0 ± 0.045		
	333	0.998 ± 0.0011	810.0 ± 11.08	− 23.3 ± 0.038		
TBOT	303	0.999 ± 0.0001	5133 ± 415.7	− 31.6 ± 0.200	90.7 ± 4.57	− 4.4 ± 1.67
	313	0.999 ± 0.0005	6093 ± 405.4	− 33.1 ± 0.386		
	323	0.999 ± 0.0010	4582 ± 613.3	− 33.4 ± 0.358		
	333	0.997 ± 0.0003	3012 ± 28.77	− 34.6 ± 0.026		
TBTT	303	0.999 ± 0.0001	5963 ± 523.3	− 32.0 ± 0.225	87.1 ± 4.7	− 5.3 ± 1.5
	313	0.998 ± 0.0004	3951 ± 858.9	− 32.0 ± 0.522		
	323	0.999 ± 0.0002	5382 ± 661.7	− 33.8 ± 0.341		
	333	0.999 ± 0.0005	4334 ± 554.2	− 34.3 ± 0.368		
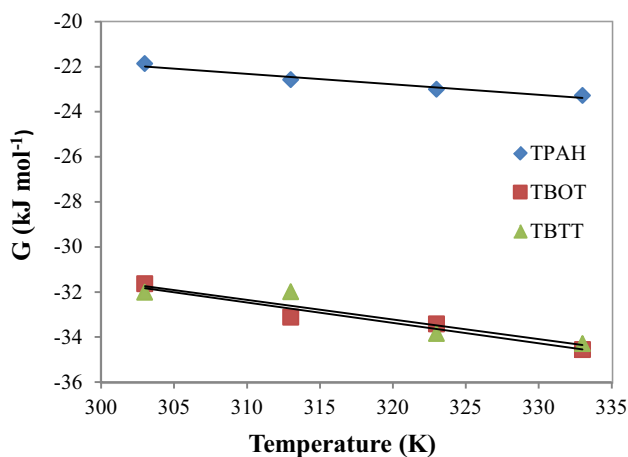
Fig. 6 Plot of ΔG_{ads} versus T for the inhibitors

observed. This indicates some complexity in the adsorption of TPAH on MS electrode. The value of n is lower (0.728) in 0.5 HCl due to irregularities and arbitrary distribution of current on the electrode surface. As the adsorption of inhibitors on the electrode surface gets more uniform n value increases. When the concentration of inhibitors increases the capacitive behavior increases as the ideal capacitor value of n is 1. Double-layer capacitance (C_{dl}) was calculated using following equation:

$$C_{dl} = \left(Y_o R_{ct}^{1-n}\right)^{1/n} \tag{11}$$

C_{dl} value decreased after the addition of any of the inhibitors. The decrease in C_{dl} with increase in concentration of inhibitors is due to replacement of H$_2$O molecules by the

Table 4 Impedance parameters for the corrosion of MS in 0.5 M HCl in the absence and presence of different concentrations of TPAH, TBOT and TBTT at 303 K

Inhibitor	Concentration (mM)	R_{ct} (Ω cm^2)	Y_o (μ Ω^{-1} s^n)	R_s (Ω cm^2)	n	C_{dl} (μF cm^{-2})	IE (%)
	Blank	198.9	356.6	22.39	0.7282	132.8	–
TPAH	1.2	338	257.2	4.67	0.7389	108.4	41.2
	2.4	436.3	213.5	4.61	0.7445	94.54	54.4
	3.6	557.5	184.6	4.57	0.7479	84.73	64.3
	4.8	877.4	122.5	17.58	0.7706	63.06	77.3
TBOT	1.2	806.9	75.97	17.12	0.8482	46.09	75.4
	2.4	933.5	73.25	17.17	0.8508	45.76	78.7
	3.6	1289	70.19	17.21	0.8521	46.25	84.5
	4.8	1589	68.91	20.57	0.8558	47.47	87.5
TBTT	1.2	1301	81.28	20.34	0.8458	53.96	84.7
	2.4	1466	73.08	20.27	0.8506	49.36	86.4
	3.6	1552	71.19	15.77	0.8513	48.45	87.2
	4.8	1613	68.74	20.61	0.8560	47.48	87.7

Fig. 7 **a** Nyquist plot, **b** bode modulus plot, **c** phase angle plot in the absence and presence of different concentrations of TPAH
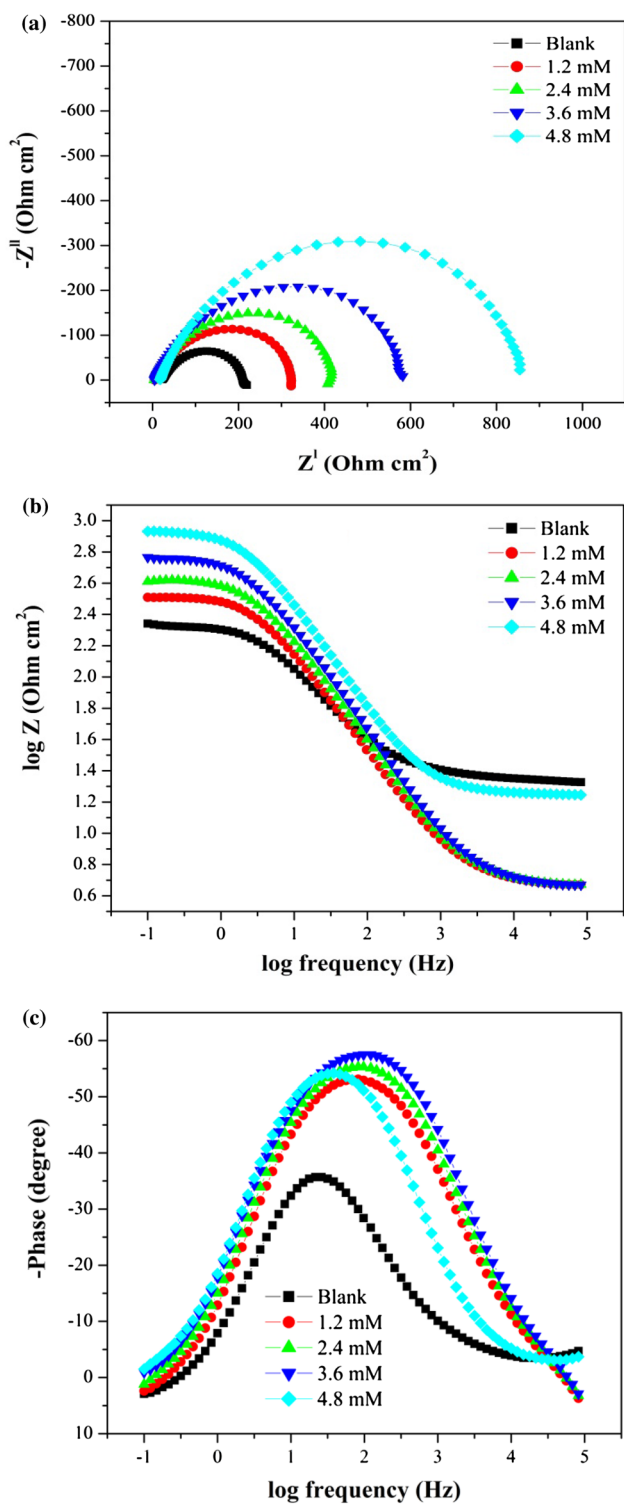

Fig. 8 **a** Nyquist plot, **b** bode modulus plot, **c** phase angle plot in the absence and presence of different concentrations of for TBOT

inhibitors resulting in the build-up of protective layer until it reaches saturation. The trend in decrease in C_{dl} for TPAH and TBTT is regular nature. TBOT exhibited irregularity
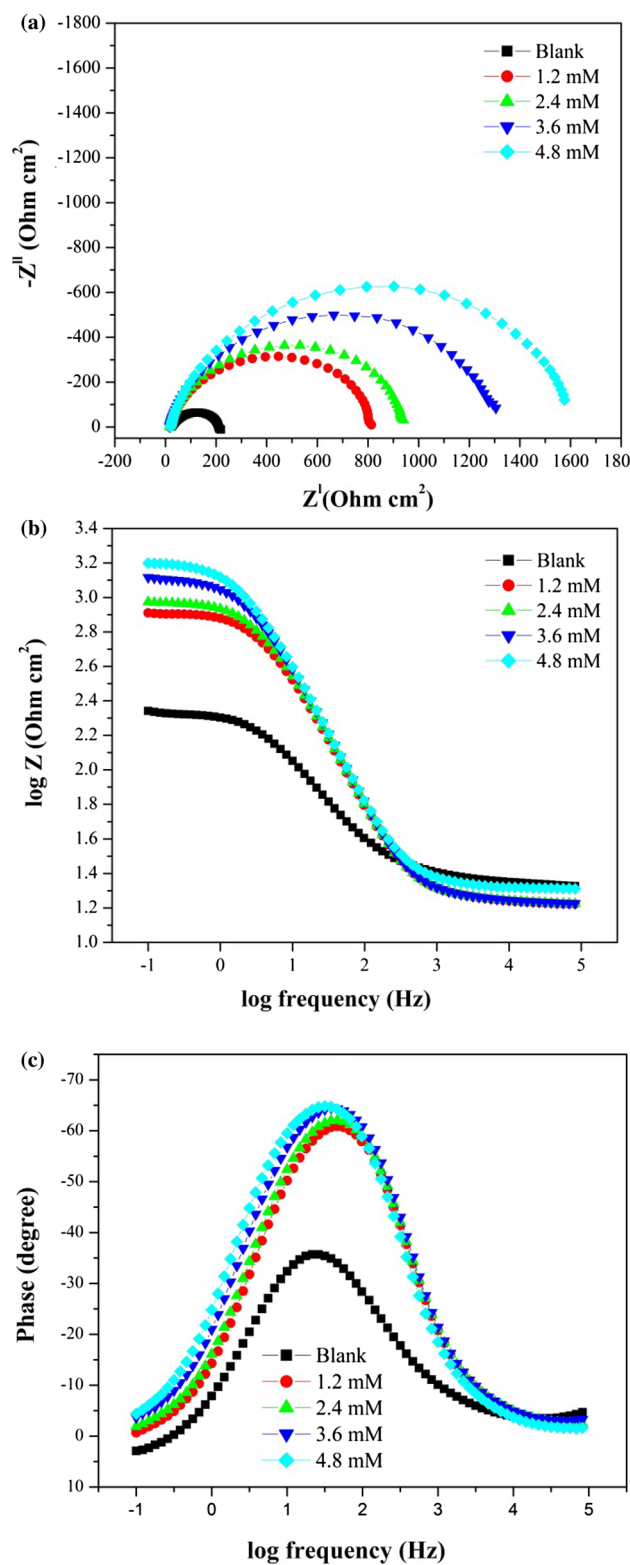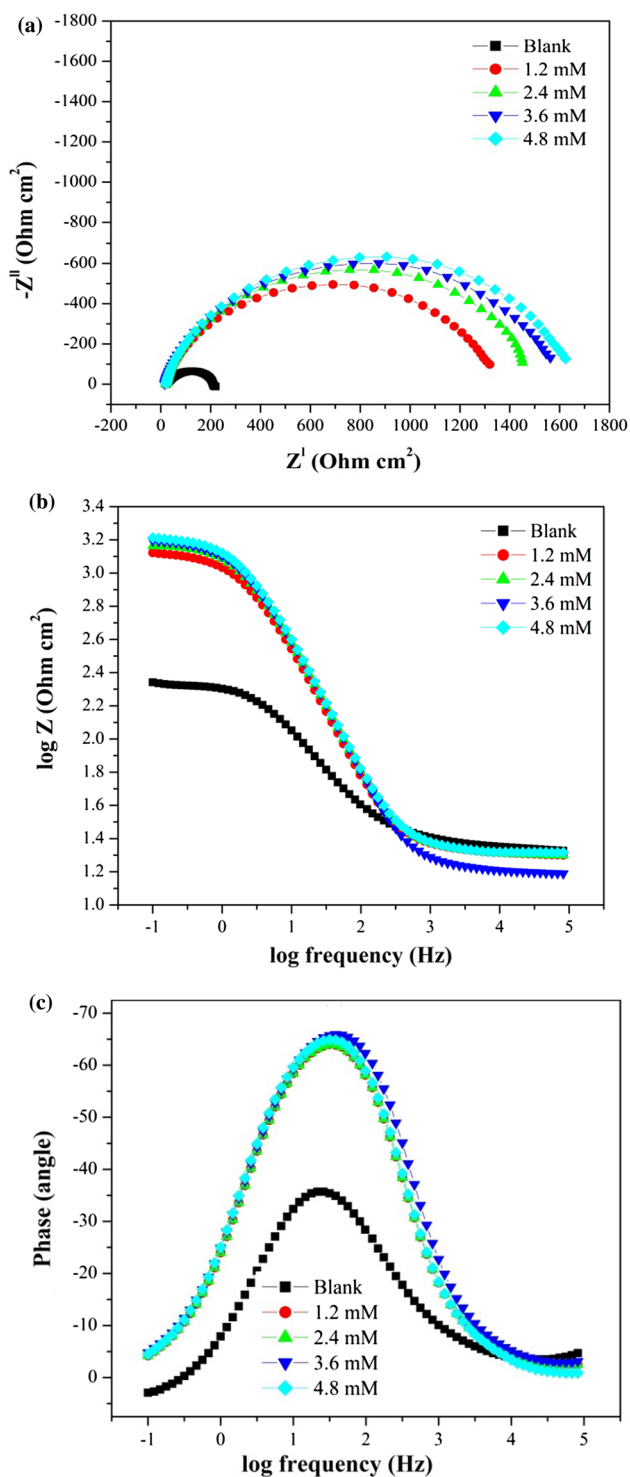
(a)

(b)

(c)

Fig. 9 **a** Nyquist plot, **b** bode modulus plot, **c** phase angle plot in the absence and presence of different concentrations of for TBTT

supporting complex adsorption–desorption process. Many reported inhibitors exhibited similar behavior [30].

From the single peak obtained in Bode plots for TPAH, TBOT and TBTT (7b, c, 8b, c, 9b, c), the electrochemical
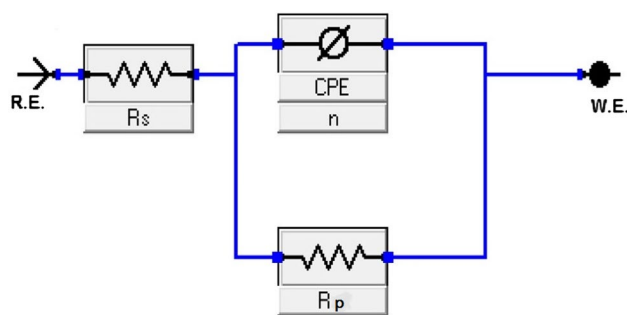
Fig. 10 Equivalent circuit model

impedance measurements fit into one time constant equivalent model. There is shift in phase maximum after the addition of inhibitors varied between 60° and 70° for the three inhibitors but the ideal capacitor will have phase maximum of 90°.

3.3 Potentiodynamic Polarization

Potentiodynamic polarization curves of MS in 0.5 M HCl containing various concentrations of TPAH, TBOT and TBTT are shown in Fig. 11. Tafel curves show that the inhibitors have considerable effect on anodic and cathodic reactions causing decrease in C_R. As anodic and cathodic domains possess linear Tafel region, the linear segments of anodic and cathodic curves were extrapolated to corrosion potential to get corrosion current densities. Electrochemical parameters, such as corrosion potential (E_{corr}), corrosion current density (i_{corr}), anodic Tafel slope (b_a), cathodic Tafel slope (b_c), are listed in Table 5.

Inhibition efficiency (IE %) can be calculated from the corrosion current density (i_{corr}) by the following equation:

$$IE\,(\%) = \frac{i_{corr}^{o} - i_{corr}}{i_{corr}^{o}} \times 100 \tag{12}$$

where i_{corr}^{o} and i_{corr} are uninhibited and inhibited corrosion current densities, respectively. There is a decrease in i_{corr} after the addition of TPAH, TBOT and TBTT, and the IE (%) is more pronounced with the increase in concentration of inhibitors. Although TBOT and TBTT exhibited good inhibition but, the highest IE (%) of 93% was exhibited by TBTT. Higher efficiency shown by TBTT as compared to TBOT is due to the presence of nitrogen atom. This is supported by general trend in the inhibition efficiencies of molecules containing heteroatoms O < N < S < P as reported by many authors [31, 32]. Shift in the values of b_a and b_c for TPAH, TBOT and TBTT indicates that inhibitors affect both cathodic and anodic reactions. The irregular trend shown in Tafel slopes may be due to many mechanisms taking part in corrosion inhibition [33]. According to Ferreira et al., if
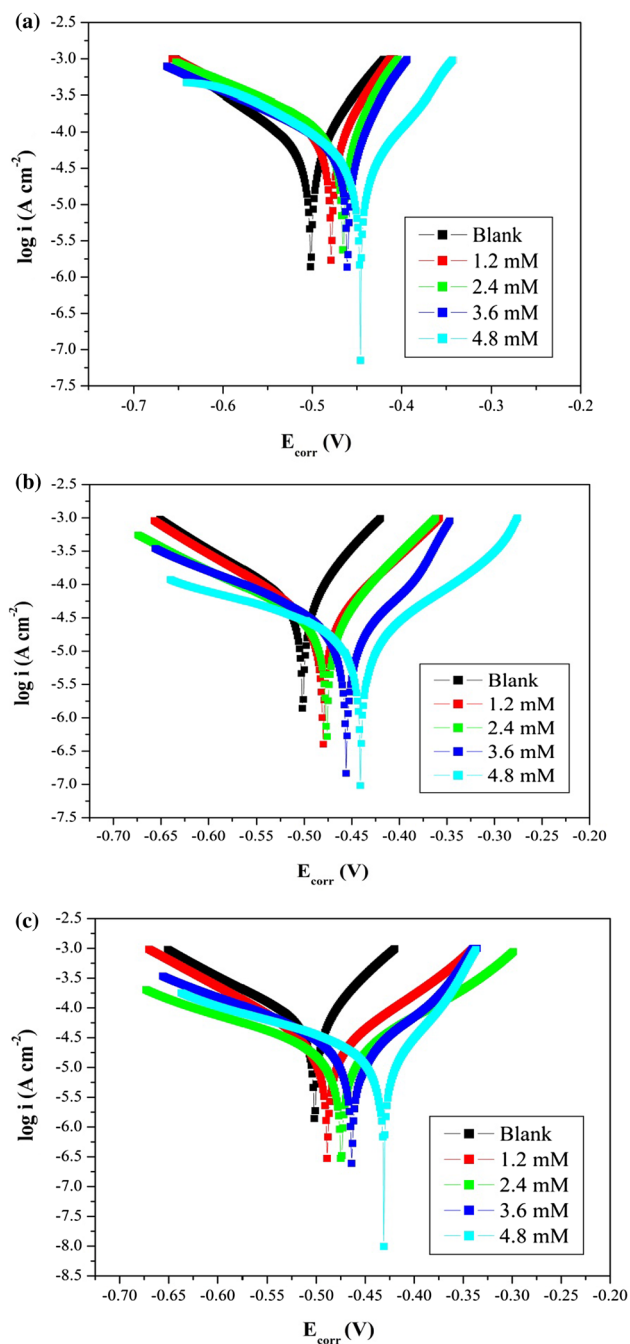
Fig. 11 Tafel plots for MS in 0.5 M HCl containing different concentration of **a** TPAH, **b** TBOT, **c** TBTT

the displacement in E_{corr} is more than 85 mV relating to the corrosion potential of the blank, then the inhibitor is considered as cathodic or anodic type. If the change in E_{corr} is less than 85 mV, then the corrosion inhibitor is regarded as mixed type [34]. The shift in E_{corr} is positive, and the maximum shift for TPAH, TBOT and TBTT is 56, 61 and 71 mV, respectively. So, all the three inhibitors are of mixed type. Since the shift in b_a is more as compared to b_c and E_{corr}

shows anodic shift, metallic dissolution is more affected than hydrogen evolution.

3.4 Quantum Chemical Calculations

The results obtained by gravimetric and electrochemical investigations can be effectively justified through quantum chemical calculations because it is a quantitative study of relationship between IE (%) and molecular reactivity. Parameters like energy of highest occupied molecular orbital (E_{HOMO}), energy of lowest unoccupied molecular orbital (E_{LUMO}), energy gap (ΔE), hardness (η), softness (σ) and electron affinity (A), that directly influence the electronic interaction of inhibitors with MS surface have been studied and they are listed in Table 7. Optimized geometrical configurations of TPAH, TBOT and TBTT are shown in Table 6. Electron densities of all the inhibitors are distributed throughout the molecules but concentrated maximum on aromatic electrons of benzene ring, triazole ring of TBTT and oxadiazole ring of TBOT indicating that these are the favorite sites for adsorption. The reactive ability of an inhibitor is closely related greater its frontier molecular orbital (FMO). Molecules with higher values of E_{HOMO} often show greater tendency for the donation of electron, enhancing the inhibitor adsorption on MS thereby giving better IE (%), whereas molecules with lower E_{LUMO} have better ability to accept electrons [35]. Also molecules with low energy gap are more polarizable and are associated with high chemical reactivity and low kinetic stability. Hence, ΔE is frequently used to characterize the binding ability of inhibitors on to the metal surface [36]. In the present study, E_{LUMO} and ΔE are more appropriate parameters to interpret IE (%). E_{LUMO} of three inhibitors varies in the order TPAH > TBOT > TBTT, and IE (%) varies in the reverse order. As TBTT has better capacity to accept electrons which helps in back donation, it is considered as the best inhibitor. ΔE of TBTT is lower than the other two inhibitors; therefore, it has better adherence capacity to the MS surface acts as the best inhibitor. Many researchers considered the negative sign of E_{HOMO} as physisorption [37, 38]. As all three inhibitors have negative E_{HOMO}, they may undergo physisorption more predominantly. Dipole moment is the resultant of non-uniform distribution of charges in atoms of inhibitor molecules. With the increase in dipole moment, the energy of deformability also increases so molecule easily gets adsorbed at the Fe surface [39]. In the present study, dipole moment follows the order TBTT > TBOT > TPAH, and IE (%) also follows the same order.

Chemical hardness basically defines the resistance toward deformation or polarization of the electron cloud of the atoms, ions or molecules under small perturbation of chemical reaction, so hard molecules have greater ΔE and a soft molecules have lower ΔE [40]. For simplest electron

Table 5 Potentiodynamic polarization parameters for the corrosion of MS in 0.5 M HCl in the absence and presence of different concentrations of TPAH, TBOT and TBTT at 303 K

Inhibitor	Concentration (mM)	E_{corr} (mV)	i_{corr} (mA cm^{-2})	b_a (mV dec^{-1})	b_c (mV dec^{-1})	IE (%)
	Blank	− 502	0.2	220	376	
TPAH	1.2	− 479	0.1165	76.6	189.1	41.7
	2.4	− 466	0.1020	67.5	178.8	49.0
	3.4	− 461	0.0641	57.8	174.4	68.0
	4.8	− 446	0.0408	80.3	147.7	79.6
TBOT	1.2	− 480	0.0308	82.5	120.3	84.6
	2.4	− 476	0.0271	71.6	153.6	86.5
	3.4	− 456	0.0166	77.3	156.3	91.7
	4.8	− 441	0.0158	95.8	206.6	92.1
TBTT	1.2	− 489	0.0217	93.7	108.2	89.2
	2.4	− 475	0.0182	100.4	189.3	90.9
	3.4	− 464	0.0172	78.3	151.5	91.4
	4.8	− 431	0.0139	61.9	196.8	93.0

transfer, adsorption occurs at that part of the molecule where softness is of highest value [41]. In the present study, TBTT has lowest hardness value and highest value of softness value so it is the best among the three studied inhibitors. It is well known that molecules with high electron affinity are highly reactive. In the present study, electron affinity shows the order TBTT > TBOT > TPAH; therefore, IE (%) follows the same order.

3.5 Scanning Electron Microscope

The micrographs of MS surface before and after immersion in 0.5 M HCl without and with addition of 4.8 mM of TPAH, TBOT and TBTT for 6 h at 303 K are shown in Fig. 12a–e. Specimens immersed in plain acid are having highly irregular surface with pits. Due to adsorption of inhibitors, the steel surface became smooth and undamaged (Fig. 12c–e), so surface properties are enhanced.
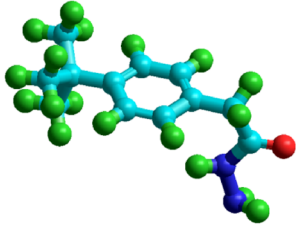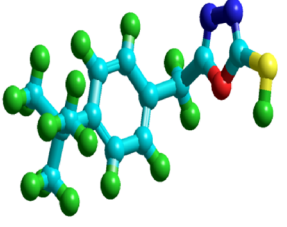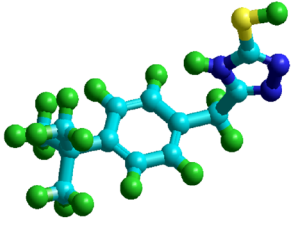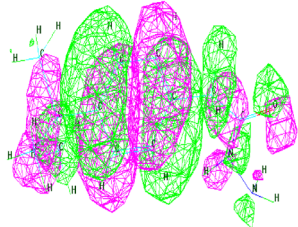
3.6 Mechanism of Inhibition
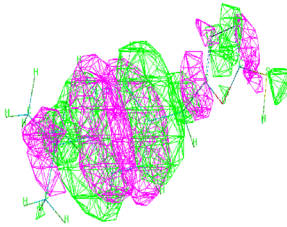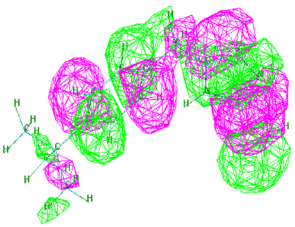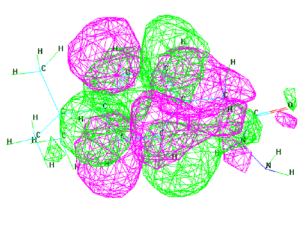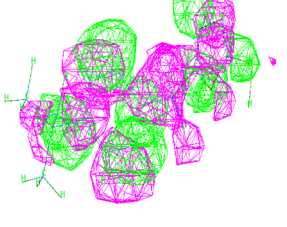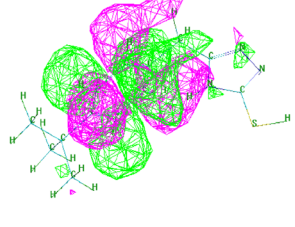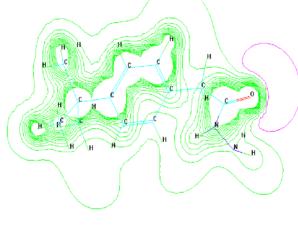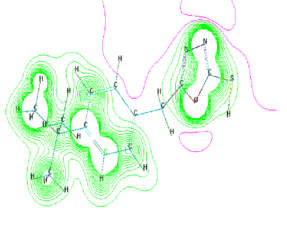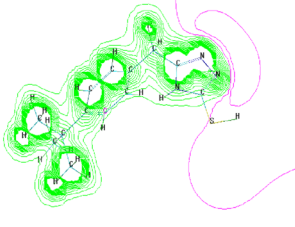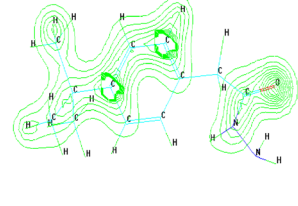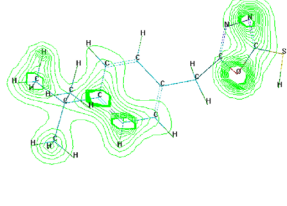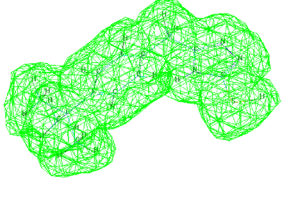
Inhibition mechanism can be proposed on the basis of mode of adsorption of TPAH, TBOT and TBTT on the steel surface. In acidic medium, both carbonyl group and nitrogen atom of TPAH can undergo protonation. From electrostatic potential map (Table 7), as more negative charge is accumulated near oxygen atom (indicated by red line) protonation of carbonyl group is more favorable. The protonation of nitrogen in TBTT and oxygen in TBOT can occur but not easy. After protonation, adsorption of positively charged inhibitors occurs on the steel surface through negatively charged chloride ions. The protonated form of inhibitors starts competing with H$^+$ for electrons on the steel surface. But, after the evolution of hydrogen gas, inhibitors come back to neutral form and prefer to get adsorbed to the MS

surface through chemisorption. Now, adsorption takes place through lone pair of electrons on nitrogen, sulfur and oxygen along with aromatic electrons through coordinate bond to the *d*-orbitals of Fe. All the three inhibitors contain electron-rich tert-butyl group, whereas TBOT and TBTT contain thiol group which increases the electron density on the aromatic system. Accumulation of excess negative charge on Fe may also result in the reterodonation of electrons to Π^* antibonding orbitals of inhibitor molecules [42]. TBOT and TBTT show better performance than TPAH due to the presence of heterocyclic ring and electron-rich thiol group. TBTT shows slightly better performance compared to TBOT because of the presence of nitrogen atom in the additional ring in the place of oxygen.

4 Conclusion

Molecules containing tert-butyl benzyl groups showed good inhibition effect on MS in acid media. The order of inhibition effect is TBTT < TBOT < TPAH. The highest IE (%) of the inhibitors at optimum concentration is 80.1, 91.7 and 92.6 for TPAH, TBOT and TBTT, respectively. From the thermodynamic and kinetic parameters obtained from the studies, the reaction between the MS and the corrosion inhibitors was spontaneous since the Gibbs free energy of adsorption values was negative. Inhibitors adsorb on the MS surface by the combination of physical and chemical adsorption with slight predominance of physisorption. Adsorption of TPAH followed Freundlich isotherm, whereas TBOT and TBTT followed Langmuir isotherm. Addition of inhibitors increased polarization resistance which and decreased double-layer capacitance and corrosion current that shows decrease in corrosion rate. Quantum chemical data revealed that inhibitors

Table 6 Optimized geometrical configurations of TPAH, TBOT and TBTT

Quantum chemical structure	TPAH	TBOT	TBTT
Optimized geometry			
HOMO			
LUMO			
Electrostatic potential map			
Total charge density			

possess sufficient electron density to have interaction with metal surface. Quantum chemical parameters like E_{LUMO}, energy gap, dipole moment and hardness confirmed the superior performance of TBTT as compared to TPAH and TBOT. As all the three methods confirmed the effective binding of studied inhibitors, they can be effectively used to prevent corrosion.
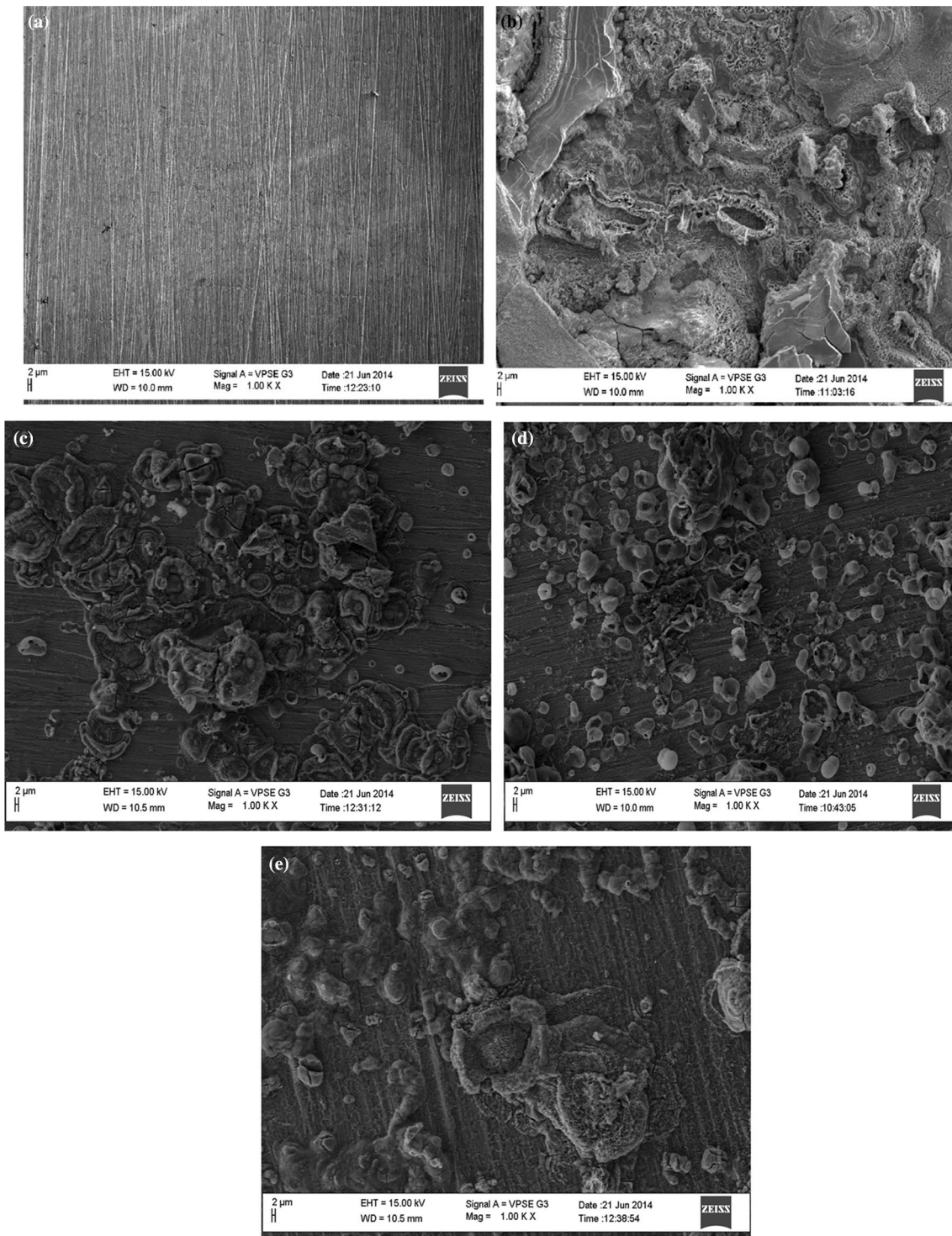
Fig. 12 SEM images of MS surface, **a** polished, **b** immersed in 0.5 M HCl, **c** immersed in 0.5 M HCl in the presence 4.8 mM of TPAH, **d** immersed in 0.5 M HCl in the presence 4.8 mM of TBOT, **e** immersed in 0.5 M HCl in the presence 4.8 mM of TBTT

Table 7 List of quantum chemical parameters for TPAH, TBOT and TBTT

Quantum chemical parameters	TPAH	TBOT	TBTT
Total energy (kJ mol^{-1})	-1.70×10^6	-2.84×10^6	-2.79×10^6
Electronic kinetic energy (kJ mol^{-1})	1.70×10^6	2.84×10^6	2.79×10^6
Nuclear repulsion energy	2.58×10^6	3.27×10^6	3.29×10^6
RMS gradient (kJ mol^{-1} Ang^{-1})	4.1754	4.4605	2.9350
Dipole (debyes)	3.2508	4.7850	5.4845
E_{HOMO} (eV)	-8.7913	-8.8036	-8.9138
E_{LUMO} (eV)	3.6026	3.5972	3.4503
$\Delta E = E_{LUMO} - E_{HOMO}$ (eV)	12.400	12.400	12.3641
Electron affinity, $A = -E_{LUMO}$	-3.6026	-3.5972	-3.4503
Hardness of the molecule (η)	6.2000	6.2000	6.1820
Softness (σ)	0.1612	0.1612	0.1617

Compliance with Ethical Standards

Conflict of interest All authors declare that they have no conflict of interest.

References

1. Eddy NO, Stoyanov SR, Ebenso EE (2010) Fluoroquinolones as corrosion inhibitors for mild steel in acidic medium; experimental and theoretical studies. Int J Electrochem Sci 5:1127–1150
2. Migahed MA (2005) Electrochemical investigation of the corrosion behaviour of mild steel in 2 M HCl solution in presence of 1-dodecyl-4-methoxy pyridinium bromide. Mat Chem Phys 93:48–53
3. Zunita M, Wahyuningrum D, Buchari Bundjali B (2012) Investigation of corrosion inhibition activity of 3-butyl-2,4,5-triphenylimidazole and 3-butyl-2-(2-butoxyphenyl)-4,5-diphenylimidazole toward carbon steel in 1% NaCl solution. Int J Electrochem Sci 7:3274–3288
4. Bouklah M, Hammouti B, Benkaddour M, Benhadda T (2005) Thiophene derivatives as effective inhibitors for the corrosion of steel in 0.5 m H_2SO_4. J Appl Electrochem 35:1095–1101
5. Achary G, Sachin HP, Naik YK, Venkatesha TV (2008) The corrosion inhibition of mild steel by 3-formyl-8-hydroxy quinoline in hydrochloric acid medium. Mater Chem Phys 107:44–50
6. Karthik R, Vimaladevi G, Chen S, Elangovan A, Jeyaprabha B, Prakash P (2015) Corrosion inhibition and adsorption behavior of 4–amino-acetophenone pyridine 2-aldehyde in 1 M hydrochloric acid. Int J Electrochem Sci 10:4666–4681
7. Quraishi MA, Sardar R, Jamal D (2001) Corrosion inhibition of mild steel in hydrochloric acid by some aromatic hydrazides. Mat Chem Phys 71:309–313
8. Larabi L, Harek Y, Benali O, Ghalem S (2005) Hydrazide derivatives as corrosion inhibitors for mild steel in 1 M HCl. Prog Org Coat 54:256–262
9. Benabdellah M, Hammouti B, Warthan A, Al-Deyab SS, Jama C (2007) 2,5-Disubstituted 1,3,4-oxadiazole derivatives as effective inhibitors for the corrosion of mild steel in 2 M H_3PO_4 solution. Int J Electrochem Sci 7:3489–3500
10. Ouici HB, Benali O, Harek Y, Larabi L, Hammouti B, Guendouzi A (2013) The effect of some triazole derivatives as inhibitors for the corrosion of mild steel in 5% hydrochloric acid. Res Chem Intermed 39:3089–3103
11. Gurudatt DM, Mohana KN (2014) Synthesis of new pyridine based 1,3,4-oxadiazole derivatives and their corrosion inhibition performance on mild steel in 0.5 m hydrochloric acid. Ind Eng Chem Res 53:2092–2105
12. Chaitra TK, Mohana KN, Tandon HC (2015) Thermodynamic, electrochemical and quantum chemical evaluation of some triazole Schiff bases as mild steel corrosion inhibitors in acid media. J Mol Liq 211:1026–1038
13. Maxwell JR, Wasdahl DA, Wolfson AC (1984) Synthesis of 5-aryl-2h-tetrazoles, 5-aryl-2h-tetrazole-2-acetic acids, and [(4-phenyl-5-aryl-4h-1,2,4-triazol-3-yl)thio]acetic acids as possible superoxide scavengers and anti-inflammatory agents. J Med Chem 27:1565–1570
14. Tomi IHR, Al-Qaisi AHJ (2011) Synthesis, characterization and effect of bis-1,3,4-oxadiazole rings containing glycine moiety on the activity of some transferase enzymes. J King Saud Univ 23:23–33
15. Agrawal R, Pancholi SS (2011) Synthesis, characterization and evaluation of antimicrobial activity of a series of 1,2,4-triazoles. Der Pharma Chem 3:32–40
16. Bentiss F, Lebrini M, Legrenee M (2005) Thermodynamic characterization of metal dissolution and inhibitor adsorption processes in mild steel/2,5-bis(n-thienyl)-1,3,4-thiadiazoles/hydrochloric acid system. Corros Sci 47:2915–2931
17. Ebenso EE (2003) Synergistic effect of halide ions on the corrosion inhibition of aluminium in H_2SO_4 using 2-acetylphenothiazine. Mat Chem Phys 79:58–70
18. Vracar L, Drazic DM (2002) Adsorption and corrosion inhibitive properties of some organic molecules on iron electrode in sulfuric acid. Corros Sci 44:1669–1680
19. Guan NM, Xueming L, Fei L (2004) Synergistic inhibition between o-phenanthroline and chloride ion on cold rolled steel corrosion in phosphoric acid. Mater Chem Phys 86:59–68
20. Singh AK (2010) Inhibiting effects of 5-substituted isatin-based Mannich bases on the corrosion of mild steel in hydrochloric acid solution. J Appl Electrochem 40:1293–1306
21. Noor EA (2009) Evaluation of inhibitive action of some quaternary N-heterocyclic compounds on the corrosion of Al–Cu alloy in hydrochloric acid. Mater Chem Phys 114:533–541
22. Umoren SA, Gasem ZM, Obot IB (2013) Natural products for material protection: inhibition of mild steel corrosion by date palm seed extracts in acidic media. Ind Eng Chem Res 52:14855–14865
23. Behpour M, Ghoreishi SM, Soltani N, Salavati-Niasari M, Hamadanian M, Gandomi A (2008) Electrochemical and theoretical investigation on the corrosion inhibition of mild steel by

thiosalicylaldehyde derivatives in hydrochloric acid solution. Corros Sci 50:2172–2181

24. Bentiss F, Legrenee M, Traisnel M, Hornez JC (1999) The corrosion inhibition of mild steel in acidic media by a new triazole derivative. Corros Sci 41:789–803

25. Martinez S, Stern I (2002) Thermodynamic characterization of metal dissolution and inhibitor adsorption processes in the low carbon steel/mimosa tannin/sulfuric acid system. Appl Surf Sci 199:83–89

26. Gopi D, Sherif EM, Manivannan V, Rajeshwari D, Surendiran M, Kavitha L (2014) Corrosion inhibition of mild steel in groundwater at different temperatures by newly synthesized benzotriazole and phosphono derivatives. Ind Eng Chem Res 53:4286–4294

27. Motamedi M, Tehrani-Bagha AR, Mahdavian MA (2011) Comparative study on the electrochemical behavior of mild steel in sulfamic acid solution in the presence of monomeric and gemini surfactants. Electrochim Acta 58:488–496

28. Ahamed I, Prasad R, Quraishi MA (2010) Experimental and theoretical investigations of adsorption of fexofenadine at mild steel/hydrochloric acid interface as corrosion inhibitor. J Solid State Electrohem 14:2095–2105

29. Singh AK (2012) Inhibition of mild steel corrosion in hydrochloric acid solution by 3-(4-((Z)-Indolin-3-ylideneamino) phenylimino) indolin-2-one. Ind Eng Chem Res 51:3215–3223

30. Karthik R, Muthukrishnan P, Chen S, Jeyaprabha B, Prakash P (2015) Anti-corrosion inhibition of mild steel in 1 M hydrochloric acid solution by using tiliacoraaccuminata leaves extract. Int J Electrochem Sci 10:3707–3725

31. Quafsaoui W, Blanc CH, Bebere N, Srhiri A, Mankowski G (2000) Study of different triazole derivative inhibitors to protect copper against pitting corrosion. J Appl Electrochem 30:959–966

32. Obot IB, Obi-Egbedi NO (2011) Anti-corrosive properties of xanthone on mild steel corrosion in sulphuric acid: experimental and theoretical investigations. Curr Appl Phys 11:382–390

33. Dubey AK, Singh G (2007) Corrosion inhibition of mild steel using Brij-30. Port Electrochim Acta 25:205–219

34. Ferreira ES, Giancomlli C, Giacomlli FC, Spinelli A (2004) Evaluation of the inhibitor effect of L-ascorbic acid on the corrosion of mild steel. Mater Chem Phys 83:129–134

35. Udhayakala P, Rajendiran TV, Gunasekaran S (2012) Theoretical approach to the corrosion inhibition efficiency of some pyrimidine derivatives using DFT method. J Comput Methods Mol Des 2:1–15

36. Ayta A, Bilgic S, Gece G, Ancin N, Oztas SG (2012) Experimental and theoretical study of the inhibition effects of some Schiff bases as corrosion inhibitors of aluminium in HCl. Mater Corros 63:729–734

37. Yurt A, Ulutas S, Dal H (2006) Electrochemical and theoretical investigation on the corrosion of aluminium in acidic solution containing some Schiff bases. Appl Surf Sci 253:919–925

38. Ashassi-Sorkhabi H, Shabani B, Aligholipour B, Seifzadeh D (2006) The effect of some Schiff bases on the corrosion of aluminum in hydrochloric acid solution. Appl Surf Sci 252:4039–4047

39. Udhayakala P, Jayanthi A, Rajendiran TV (2011) Adsorption and quantum chemical studies on the inhibition potentials of some formazan derivatives. Der Pharma Chem 3:528–539

40. Obi-Egbedi NO, Obot IB, El-Khaiary MI, Umoren SA, Ebenso EE (2011) Computational simulation and statistical analysis on the relationship between corrosion inhibition efficiency and molecular structure of some phenanthroline derivatives on mild steel surface. Int J Electrochem Sci 6:5649–5675

41. Hasanov R, Sadikglu M, Bilgic S (2007) Electrochemical and quantum chemical studies of some Schiff bases on the corrosion of steel in H_2SO_4 solution. Appl Surf Sci 253:3913–3921

42. Ansari KR, Yadav DK, Ebenso EE, Quraishi MA (2012) Novel and effective pyridyl substituted 1,2,4-triazole as corrosion inhibitor for mild steel in acid solution. Int J Electrochem Sci 7:4780–4799